JOURNAL OF AIRCRAFT
Vol. 42, No. 6, November–December 2005

Numerical Simulation of Icing Clouds in the NASA Glenn Icing Research Tunnel

C. Bhargava* and E. Loth†
University of Illinois at Urbana–Champaign, Urbana, Illinois 61801
and
M. Potapczuk‡
NASA John H. Glenn Research Center at Lewis Field, Cleveland, Ohio 44135

The objective of this study was to develop and employ a numerical simulation strategy for predicting the liquid water content (LWC) at the test-section plane of the NASA Glenn Icing Research Tunnel (IRT) as well as to characterize the icing cloud uniformity as a function of tunnel speed, droplet size, etc. The droplets were injected with a polydisperse distribution and based on previous computational airflow results, which included the spray-bar wakes, the air jets, and the heat-exchanger flow. To simulate the effects of turbulent diffusion behavior of water droplets in the IRT, a continuous-random-walk methodology was employed, which corrects for nonhomogeneous turbulence. To first understand the cloud dynamics emanating from isolated nozzles, experiments and simulations were conducted with only four injectors spraying in the IRT. The simulations showed good representation of the width and position (though not necessarily the shape) of the individual spray clouds at the test-section plane. Next, droplets issued by the baseline group of spray nozzles were simulated in order to determine the test-section LWC distributions which in turn were used to compare with experiments. The simulations indicated the importance of including turbulent diffusion, and that increased tunnel speed and droplet size tended to reduce overall uniformity, which was generally consistent with experimental results.

Introduction

THE Federal Aviation Administration's certification of commercial aircraft and the qualification of military aircraft each require evaluation during icing conditions. Effective ground-based simulation of icing conditions is conventionally achieved can be performed in refrigerated wind-tunnel facilities through the use of nozzles on a spray-bar system, where the water droplets are entrained in the wake of spray bars. The droplets are transported downstream by the tunnel air, reach a supercooled state from the subfreezing air temperatures, and result in a dispersed cloud at the test section. A primary consideration in generation of the icing cloud is that the test-section liquid water content (LWC) should have high spatial uniformity in order to ensure known conditions for all surfaces of a test model. Trial-and-error adjustment of nozzle and test conditions to produce a uniform cloud is a complex process. Thus, computational methods, which track the turbulent dispersion of the water droplets as they proceed from the nozzles to the test section, could be beneficial to design and/or improve the test section LWC uniformity.

Most previous droplet trajectory methodologies used for icing research tunnels have primarily considered only the mean velocity distributions within the tunnel, for example, Bragg and Khoudadoust.[1] However, it was noted by Hancir and Loth[2] that turbulent diffusion is an important factor that affects the spatial uniformity of the icing cloud. DeAngelis et al.[3] developed a two-phase algorithm that reasonably predicted turbulent dispersion of water droplets in a wind tunnel. The procedure was based on a Lagrangian transport methodology for the droplet phase and was used to study key parameters affecting the LWC in the testing section. A parametric study was completed by DeAngelis et al. to investigate the effects of computational, spray, vapor, and wind-tunnel parameters. It was found that LWC spatial deviations depend primarily on tunnel turbulence levels and secondarily on droplet temperature and velocity. Based on this technique, Hancir and Loth[2] conducted studies for the pre-1999 configuration of the NASA Lewis Icing Research Tunnel (IRT). Their results indicated that turbulence resulting from the heat exchanger (HX), spray bars, and air-jet wakes were all critical factors in modeling the droplet dispersion (whereas the wall boundary layers were not critical). However, the Hancir and Loth predictions yielded only qualitative agreement with respect to the measured test section turbulence. The lack of quantitative fidelity was attributed to the complex flow resulting from the W-geometry heat exchanger (which yielded substantial flow nonuniformities) and to the absence of the detailed flow simulation of the jet and spray-bar wake features (which were treated with simple one-dimensional empirical expressions as opposed to being predicted numerically).

The present investigation is a modification and extension of the previous computational research by Hancir and Loth[2] but for the revised NASA Glenn Research Center (GRC) IRT configuration (Fig. 1). Wind-tunnel improvements completed in 1999 included replacing the original folded heat exchanger with a more uniform planar heat exchanger, expanding the width of the tunnel loop to accept the larger flat heat exchanger, as well as adding new corner turning vanes downstream of the heat exchanger and exit guide vanes downstream of the drive fan. A portion of the revised tunnel geometry is given in Fig. 1a, which includes spray bars located just upstream of the 14:1 tunnel contraction section. Modifications to the icing facilities also included an increase in the number of air/water nozzles (at the spray bar trailing edges), with a new arrangement as shown in Fig. 1b. The spray nozzles for the IRT consist of a coaxial air-water system, identified by the tunnel personnel as the Mod-1 nozzles. The nozzle distribution was finalized after 30 iterations by Ide and Oldenburg[4] to maximize the icing cloud uniformity in the test section. Comparing the experimental data taken before and after the tunnel modifications, it was found that there was a significant improvement at the two stations[5,6] (settling chamber and test section) in terms of flow uniformity and a substantially decreased

Presented as Paper 2004-0563 at the AIAA 42nd Aerosoapce Sciences Meeting, Reno, NV, January 2004; received 28 June 2004; revision received 29 September 2004; accepted for publication 29 September 2004.

*Professor, Technical Services, Epic Systems Corporation, Madison, WI.
†Professor of Aerospace Engineering, 306 Talbot Laboratory, 104 S. Wright Street; loth@uiuc.edu.
‡Aerospace Engineer, MS 11-2, 21000 Brookpark Road.

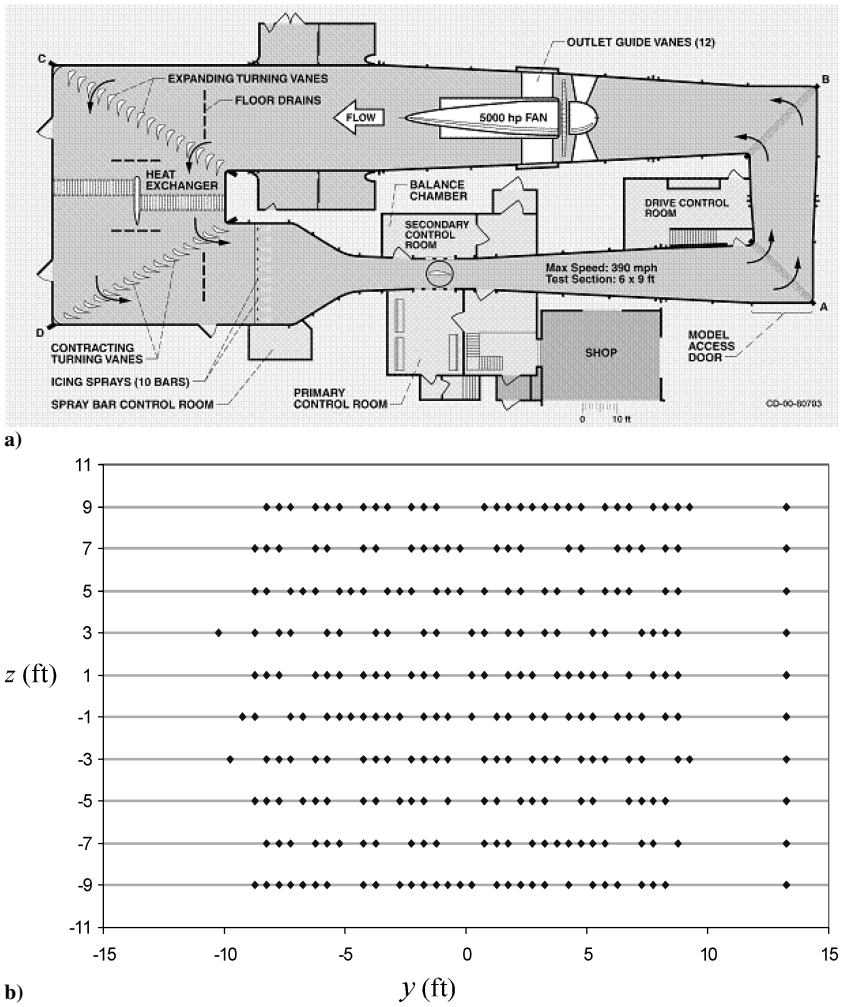

Fig. 1 Schematic of the a) IRT showing spray injector location and test section and b) spray-bar locations (——) and nozzle locations (◆ ◆).

turbulence and flow angularity in the test section. In addition, there measurements of mean velocity, turbulence levels, and the power spectrum.

Recently Bhargava et al.[7] used the shear-stress transport (SST) turbulence model (of the WIND code[8]) to simulate the airflow in the new IRT configuration from the spray bars to the test section. The simulations used experimental inflow conditions just upstream of the spray bars (in terms of mean and rms velocity in streamwise and vertical directions as well as the overall power spectrum). Unlike the Hancir and Loth studies, which used empirical models, the spray-bar wake and jet features were simulated with the SST turbulence model and then were linearly combined with the HX flow to get an overall flow description. The heat exchanger and spray-bar flow solutions provided improved predictions for the test-section aerodynamics, including the mean velocity and the turbulent-kinetic-energy distributions.

Using the airflow solution from this recent study, the objective of the present investigation is to develop a robust and accurate methodology for predicting the LWC physics and test-section uniformity for the updated IRT configuration.

Numerical Methods

In the following, we describe the particle-phase governing equations. These are based on the instantaneous surrounding-fluid velocity that the particle "sees." This fluid velocity consists of both a time-averaged mean velocity given throughout the flow domain and a random component caused by turbulence. The latter is supplied by a stochastic model to simulate the velocity fluctuations along the droplet path, thus incorporating the effect of turbulent diffusion. This random walk technique was validated using canonical turbulent flows for which the mean velocity profiles $\boldsymbol{u}_f$, as well as the distribution of the turbulent kinetic energy k and turbulent dissipation ε, are known. Note that solution of the Reynolds-averaged Navier–Stokes (RANS) airflow must be known ahead of time to apply this method. In the present study, the IRT airflow (including $\boldsymbol{u}_f$, k, ε distributions) is described in Bhargava et al.[7] The details of the trajectory technique are given in the following.

Particle-Phase Governing Equations

Droplet movement is dictated by the equations of motion for position and velocity. The position of the droplet (referred to as a "particle" in this section) can be solved by the following equation:

$$\frac{\mathrm{d}\boldsymbol{x}_p}{\mathrm{d}t} = \boldsymbol{U}_p \tag{1}$$

where $\boldsymbol{x}_p$ is the particle location and $\boldsymbol{U}_p$ is the instantaneous particle velocity vector. The particle acceleration is affected by only aerodynamic drag and gravity if the particle density is much greater than the gas density ($\rho_p \gg \rho_f$), as is the case herein. In addition, the particle loading is very small, that is, the mass and momentum flux of the droplets at any point in the domain is on the order of 0.1% of the mass and momentum flux of the airflow. As such, droplet-droplet interactions can be ignored, and droplet effects on the airflow will be negligible. Thus, the particle velocity can be found by solving a standard equation of motion for a spherical droplet of diameter d_p as

$$\frac{\mathrm{d}\boldsymbol{U}_p}{\mathrm{d}t} = \frac{3}{4}\frac{\rho_f}{\rho_p}\frac{|\boldsymbol{U}_f - \boldsymbol{U}_p|}{d_p}(\boldsymbol{U}_f - \boldsymbol{U}_p)C_D + \boldsymbol{g} \tag{2}$$

where $\boldsymbol{g}$ is the acceleration caused by gravity, C_D is the droplet drag coefficient, and the instantaneous surrounding gas velocity at the

droplet location is $\boldsymbol{U}_f$. Because all particles are considered spherical, C_D is taken to be

$$C_D = (24/Re_p)\left(1 + Re_p^{\frac{2}{3}}/6\right) \quad \text{if} \quad Re_p < 1000$$
$$= 0.424 \quad \text{otherwise} \tag{3}$$

where the particle Reynolds number is based on viscosity (μ_p)

$$Re_p = \rho_f |\boldsymbol{U}_f - \boldsymbol{U}_p| d_p/\mu_f \tag{4}$$

The particle dynamic equation is computed using a semi-implicit time-marching scheme described by Bocksell and Loth,[9] where temporal resolution is assured to be sufficient. The method for determining the turbulent fluctuations associated with $\boldsymbol{U}_f$ needed in Eq. (2) (i.e., to incorporate the effect of turbulent diffusion) is discussed in the following section.

Stochastic Eddy Model

The instantaneous gas velocity fluctuation $\boldsymbol{U}_f$ is broken up into a mean velocity and a fluctuating component

$$\boldsymbol{U}_f = \boldsymbol{u}_f + \boldsymbol{u}'_f \tag{5}$$

For the continuous-random-walk (CRW) method, a random number generator is used to simulate the stochastic instantaneous fluid velocity perturbation as seen locally by the particle $\boldsymbol{u}'_f$. This perturbation is combined with the local mean velocity vector to compute the trajectory of a statistically large number of particles in the flow to obtain the mean particle diffusion information. Thus, droplets are advected based on the combination of mean velocity and a turbulent velocity perturbation for the airflow. In Eq. (5), the mean velocity component can be simply obtained from the mean velocity distributions from a RANS solution. The fluctuating component can be simulated stochastically to have an rms variation consistent with the turbulent kinetic energy k and an average temporal decorrelation consistent with the turbulent timescale τ_Λ, both of which can be obtained from results with a conventional two-equation RANS turbulence model.

For the CRW method, a discrete Markov chain is used to correlate the continuous-phase velocity fluctuation $\boldsymbol{u}'_f$ with the value at the previous time step along the particle path. Assuming isotropic turbulence, the rms of this Markov chain for homogeneous turbulence should be consistent with the rms of the velocity fluctuations prescribed by the one-dimensional component of the turbulent kinetic energy, that is, $(2k/3)^{1/2}$. From this, the discretized Markov chain becomes (written in vector form)

$$\boldsymbol{u}'_f(t + \Delta t) = \psi \boldsymbol{u}'_f(t) + (1 - \psi^2)^{\frac{1}{2}} \boldsymbol{\gamma}(t)(2k/3)^{\frac{1}{2}} + \delta \boldsymbol{u}'_f$$
$$\psi = \exp(-\Delta t/\tau_{\text{int}}) \tag{6}$$

where ψ is the decorrelation variable, $\boldsymbol{\gamma}$ is a random number vector selected from a Gaussian distribution and sampled every time step and for each Cartesian direction, τ_{int} is the eddy-particle interaction timescale, and $\delta \boldsymbol{u}'_f$ is a correction for nonhomogeneous turbulence. Bocksell and Loth[9] noted that the time-step size constraint allowed for statistical independence of mean particle diffusion (within 1%) is $\Delta t < \tau_{\text{int}}/8$.

The interaction timescale is given by the minimum of an eddy lifetime τ_Λ and a particle-eddy transit time τ_{tr}:

$$\tau_{\text{int}} = \min(\tau_\Lambda, \tau_{\text{tr}})$$

where

$$\tau_\Lambda = c_\tau k/\varepsilon, \qquad \tau_{\text{tr}} = (\Lambda/|U_f - U_p|), \qquad \Lambda = c_\Lambda c_\mu^{\frac{3}{4}} k^{\frac{3}{2}}/\varepsilon \tag{7}$$

where Λ represents the isotropic integral eddy size and where $c_\tau = 0.124$ and $c_\Lambda = 0.78$ were determined based on calibration for the Snyder and Lumley particle diffusion data and $c_\mu = 0.09$.

This form of the interaction timescale can capture both the crossing trajectory effect (where $\tau_{\text{int}} = \tau_{\text{tr}}$) and eddy lifetime effect (where $\tau_{\text{int}} = \tau_\Lambda$) as defined by Snyder and Lumley.[10] Note $\tau_{\text{int}} \leq \tau_{\text{tr}}$ so that any crossing trajectory effects (as a result of increasing particle inertia) will reduce the interaction timescale, and thus decrease the velocity correlation. This is consistent with the fact that increasing particle size has been found to yield higher relative velocities (as a result of either terminal velocity or an inability to respond to the surrounding airflow velocity fluctuations). As such, larger particles will cause the eddy interaction to be more likely controlled by the crossing trajectory effect (and τ_{tr}), whereas smaller particles tend to be controlled by τ_Λ. Another effect is that an increase in the turbulent kinetic energy will increase particle diffusion (for a given particle inertia). These two trends can be seen from a theoretical estimate of the mean square of droplet trajectory position y'_p over some period of time t (which is much greater than τ_{int}) by Hinze[11]

$$\overline{y'^2_p} \approx \text{const}\, k \tau_{\text{int}} t \tag{8}$$

Thus the highest diffusion tends to be for the smallest drops in the highest turbulence, whereas the lowest droplet diffusion will correspond to the largest drops in the lowest turbulence. This is consistent with direct-numerical-simulation (DNS) results of Elghobashi and Truesdell[12] and the experiments by Loth and Stedl[13] as discussed by Loth.[14]

An example/validation of the prediction for transverse particle diffusion in the grid-generated wake data of Snyder and Lumley[10] (which is a nearly homogenous isotropic turbulence field) is shown in Fig. 2 using the preceding CRW model. The heavier particle yielded reduced diffusion in accordance with increased particle inertia and thus reduced turbulent interaction timescale [as noted by Eq. (7)].

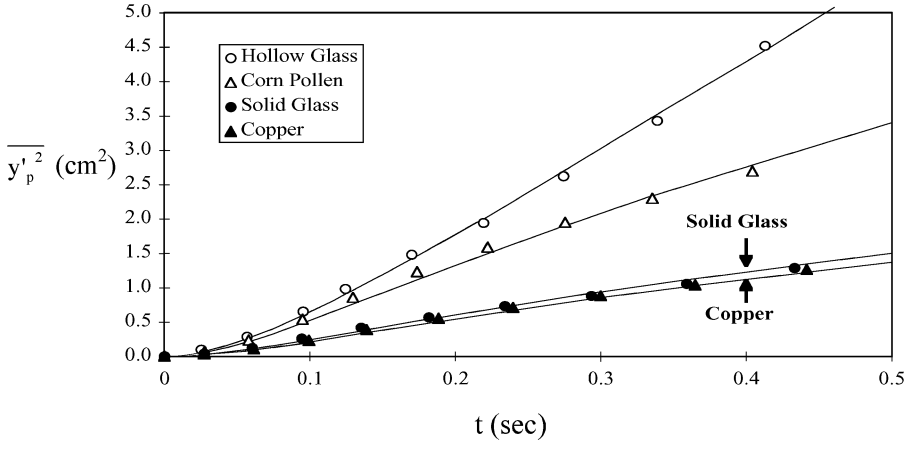

Fig. 2 Experimental and numerical mean particle diffusion in grid-generated turbulence.

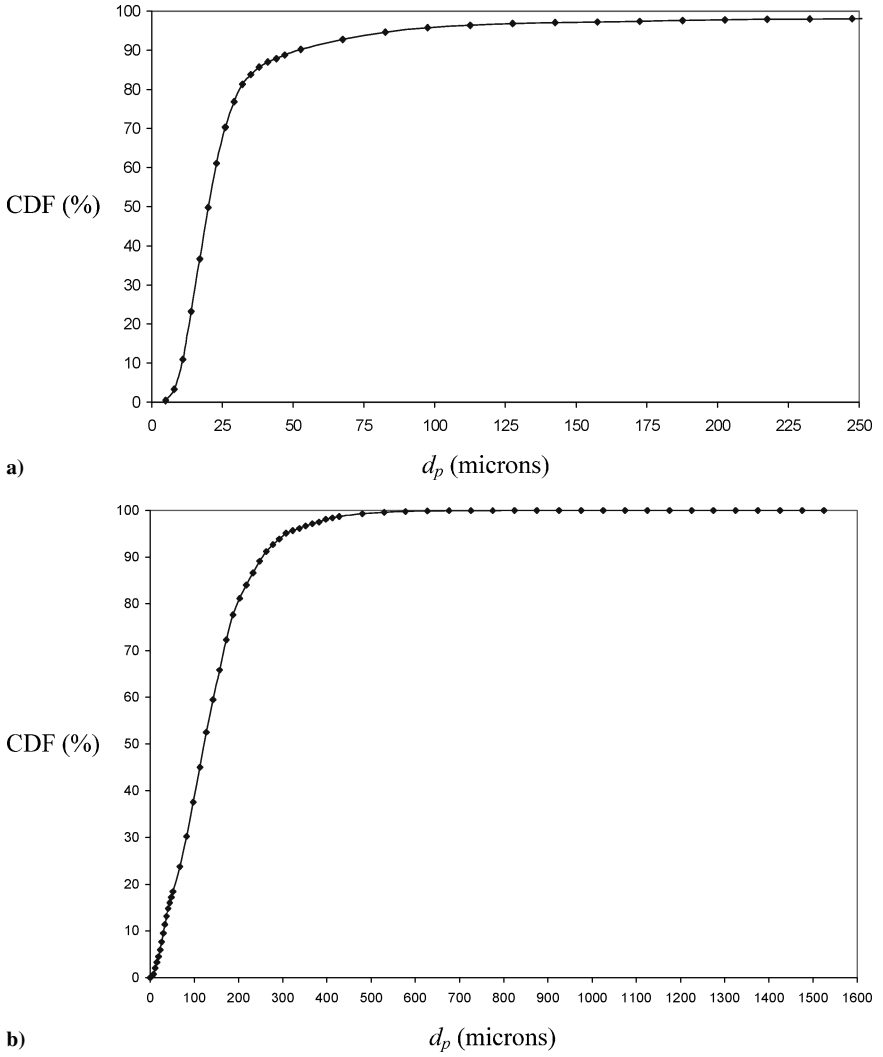

Fig. 3 Experimental data for cumulative distribution function vs diameter for MVD of a) 21 μm and b) 120 μm.

For nonhomogeneous turbulence, the last term on the right-hand side of Eq. (6) $\delta \boldsymbol{u}'_f$ is a correction needed if the particle moves across regions with gradients in the kinetic energy. The nonhomogeneous turbulence effects can be shown to provide a nonphysical "drift" in the Markov chain if not corrected. This is a result of converting an Eulerian statistical representation to a Lagrangian statistical representation. The correction is accounted for by noting the strength of the kinetic energy gradient.[9] For isotropic turbulence with no cross correlations used to create the stochastic $\boldsymbol{u}'_f$, the correction is given as

$$\delta v'_f = \Delta t \frac{1}{3} \frac{\partial k}{\partial y}, \qquad \delta w'_f = \Delta t \frac{1}{3} \frac{\partial k}{\partial z} \tag{9}$$

Applications of the preceding CRW technique for shear flows (wakes and jets) for short and long integration times (compared to τ_Λ) show that the technique provides high fidelity for mean particle diffusion despite nonhomogeneous turbulence.[9]

Droplet Polydisperse Profile

For the sprays emanating from the nozzles, the resulting droplets are not a constant diameter but instead can be characterized by a wide range of droplet sizes, from which an average droplet diameter can be determined. The cumulative distribution function (CDF) gives the fraction of mass (or LWC) contained in particles of diameter d_p or less.

Experiments at NASA Glenn Research Center (Ide, R., personal communication, 2003) identified CDF curves for clouds with a mean volumetric diameter (MVD) of 20 μm and of 120 μm (Fig. 3). It can be seen that the droplet diameter variation is substantial in both cases and thus should be taken into account for predicting droplet distributions in the test section. Using cubic splines, an interpolated curve was obtained for d_p vs CDF. To simulate this size distribution, a linear random number generator (RNG) between 0–1 with equal probability throughout the interval was obtained for each droplet injection event. The RNG value was set equal to CDF from which the interpolated function was used to determine the corresponding diameter. A statistically significant number of droplets (10,000) were injected in this manner to cover the entire CDF range and thus reproduce the same droplet diameter distribution as found in the IRT. The two MVD cases used herein allow for a stringent test of the predictive methodology as they represent a significant variation in droplet inertia (e.g., the ratio of droplet response time between the two cases is more than six-fold).

Droplet Trajectory Method for IRT

As its inputs, the droplet trajectory computer methodology requires values for the mean airflow properties as well as the turbulent kinetic energy and turbulence dissipation throughout the computational domain. In these simulations, the trajectories were computed for droplets emanating from the IRT's spray jets. The theoretical airflow velocity for a Mod-1 nozzle was used as the initial droplet velocity. The theoretical airflow value was based upon the nozzle diameter and the mass flow rate, which in turn is based on the measured difference between the jet air pressure and the jet water pressure and the continuity and momentum equations. The resulting values were

34.4 m/s for the 21-μm droplets and 28.39 m/s for the 120-μm droplets. Although there might be some uncertainty associated with this injection velocity (around 10–20%), a parametric study showed that the initial velocity of the particles had a negligible effect on the distribution of the particles in the test section. This is expected because the droplet response time is much smaller than the time for the injected particles to reach the test section so that the specification of the initial velocity is not critical.

LWC Calculations: Four Nozzles and Baseline Nozzles

The objective of this methodology is to be able to predict the cloud uniformity (not the absolute LWC). Therefore it is important to evaluate the computational capability to simulate spatial variances of the LWC in terms of the mean location and diffusion associated with injected droplets. This will be considered first with just four nozzles injecting droplets at the spray-bar location so that the individual nozzle diffusion patterns and mean trajectories can be identified and evaluated with experiment completed specifically for this purpose. This is followed by the practical case where many injectors are used (baseline nozzles) whose position and number were previously selected in order to establish a reasonably uniform test-section water droplet cloud.

The droplet trajectory code tracked the paths of the particles and recorded the particle axial velocity and location as it crossed the LWC measurement plane located in the test section (47.8 ft from settling chamber plane). The transverse and vertical locations at this plane were selected to be consistent with the experimental measurements at NASA GRC, that is, the plane was divided into equally sized bins of 15×15 cm. A secondary program collected these particles into square bins using the method of DeAngelis et al.,[3] whereby the sum of particle mass flux normalized by particle flux velocity and bin area ($m_p/u_p A_{\text{bin}}$) is proportional to the LWC of each bin. Two simulation sets were completed: a four-nozzle case and a baseline-nozzle case. The four-nozzle case specified droplet injector from four nozzle spaced significantly far from each other so that the individual nozzle clouds would not overlap. This case was investigated to understand the diffusion from a single injector as a function of drop size and tunnel speed. The baseline nozzles specified droplet injection from the approximately 100 nozzles used in the Ide and Oldenburg[4] experiments, which correspond to the best configuration for maximizing LWC uniformity in the test section. This case was considered to evaluate the predictive performance for describing LWC uniformity.

To characterize the LWC distribution at the measurement plane for the four-nozzle cases, a Gaussian distribution was fit to both the experimental LWC and the predicted LWC results for each individual nozzle's spray cloud. The Gaussian distribution was based on the equation

$$\text{LWC}_{\text{Gauss}} = L^*_{\text{peak}} \exp\left\{-\left[(y - y_{\text{peak}})^2 + (z - z_{\text{peak}})^2\right]\Big/\sigma^2\right\} \quad (10)$$

where $\text{LWC}_{\text{Gauss}}$ is the value of LWC obtained using Gaussian fit and where L_{peak} is the maximum value of LWC (experimental or predicted), y_{peak} and z_{peak} are the horizontal distance (from the center of the test section) and the vertical distance (from the lower tunnel wall) to the peak LWC location for a given cloud, and σ is the Gaussian width of the LWC cloud. To simultaneously determine these parameters, an optimized Gaussian fit was obtained for each injector cloud by minimizing the average fit error, defined as the spatial integration of the absolute difference between the actual LWC and that given by a Gaussian distribution, i.e., $|\text{LWC} - \text{LWC}_{\text{Gauss}}|_{\text{avg}}$. The L_{peak}, y_{peak}, and z_{peak} were thus obtained for each of the four individual nozzle clouds for a wind-tunnel test, whereas σ_{avg} was obtained by averaging the values for all four clouds (further details are given in Bhargava et al.[15]). Both the experimental and simulated spray cloud width, location, and magnitude were quantified in this manner so that they could be compared quantitatively.

For the case with the baseline set of injectors, the LWC at each bin was nondimensionalized by scaling with the centerline bin LWC value (for both experiments and simulations). From this, the test-section plane LWC spatial distributions could be compared.

Results

LWC for Cases with Four Nozzles

In this portion of the study, the predicted LWC distribution for four nozzles spraying was compared with that of the experimental LWC distribution [obtained by Ide (personal communication, 2003)]. The objective of this test was to understand the cloud dynamics (e.g., how turbulent diffusion is affected by droplet size and tunnel speed) and to determine whether the droplet cloud emanating from a single nozzle could be reasonably predicted (e.g., in terms of its mean location and spread at the LWC plane). The four nozzle locations for spraying (with air injection as well) were chosen at $y = \pm 57$ in. and $z = \pm 60$ in. based on previous studies (Ide, R., personal communication, 2003) so as to allow individual cloud spreading while avoiding any cloud overlap. The rest of the Mod-1 nozzles only issued air. Two sets of droplet injection conditions (MVD of 120 μm at a jet air pressure of 5 psig and with MVD of 21 μm at a jet air pressure of 20 psig) and three wind-tunnel speeds (100, 150, and 200 kn) were considered. To simulate these conditions, a total of 100,000 particles were injected.

Figure 4a shows the LWC contour plots (experimental and predicted, respectively) for the 21-μm mean diameter droplet sprays at 100 kn. For both measurements and simulations of LWC, the four nozzles created clouds about 20 in. in diameter that were roughly circular with center peaks. In addition, the mean locations of the clouds were reasonably predicted. However, there were some noncircular aspects for the measured LWC values, and these were not consistently predicted.

Figure 4b shows the same airflow conditions of 100 kn but for 120-μm MVD sprays. The result is a noticeable reduction in cloud diameter (per nozzle) to about 14 in. for both predictions and experiments. This reduced diffusion is a result of the increased inertia of the larger droplets. This leads to droplet interactions with the turbulence to be more controlled by the crossing trajectory effect (than by the eddy integral timescale), which reduces the eddy interaction time [consistent with Eq. (7)]. Though not a strong effect, the mean cloud locations are also slightly closer to the center as a result of mean path-line variations, an effect that can be predicted without incorporating turbulent diffusion models.[1]

Figures 4c and 4d are measured and predicted LWC distributions for test-section speeds of 150 and 200 kn (all for 120-μm MVD sprays with 5 psig for the nozzle airflow rate). Because the air jet pressure is the same for Figs. 4b–4d, the turbulence from the jets contribution to overall turbulent diffusion in the tunnel is approximately constant, whereas the timescale for the droplet diffusion t varies inversely to the test-section speed. It can be seen that these cases indicate that an increase in the test-section speed leads to a decrease in the individual cloud size (around 10 in. in diameter for the 200-kn condition). This behavior occurs for both measured and predicted results and is consistent with a reduced time of trajectory to the test section for nearly constant turbulence [see Eq. (8)]. In general, the clouds are also more noncircular as the tunnel speed increases, which is attributed to the concomitant increased magnitude (and thus importance) of spray-bar wake turbulence, which results in a more complex flowfield for the droplets. Experimental deviations from a Gaussian shape were not consistently observed in the computations, and the primary features were generally predicted. Similar trends and overall predictive ability were found for an increase in test-section speed for the 21-μm MVD drop cases.[16] For the mean cloud position, there is only a small change as a result of test-section velocity (consistent with the droplet trajectory being governed more by contraction geometry, mean droplet diameter, and path length).

The next set of figures compares properties obtained by making Gaussian fits to each cloud (both from measurements and simulations). This allows quantitative characterization of droplet size and tunnel speed effects on cloud dynamics (peak location, cloud width, and peak magnitude) as well as a quantifiable comparison between experiments and predictions. Figure 5 shows location of the four peak values of $\text{LWC}_{\text{Gauss}}$ (y_{peak} and z_{peak}) for both experiments and predictions at the test flow speed of 150 kn (for both droplet spray conditions). It can be seen that the larger

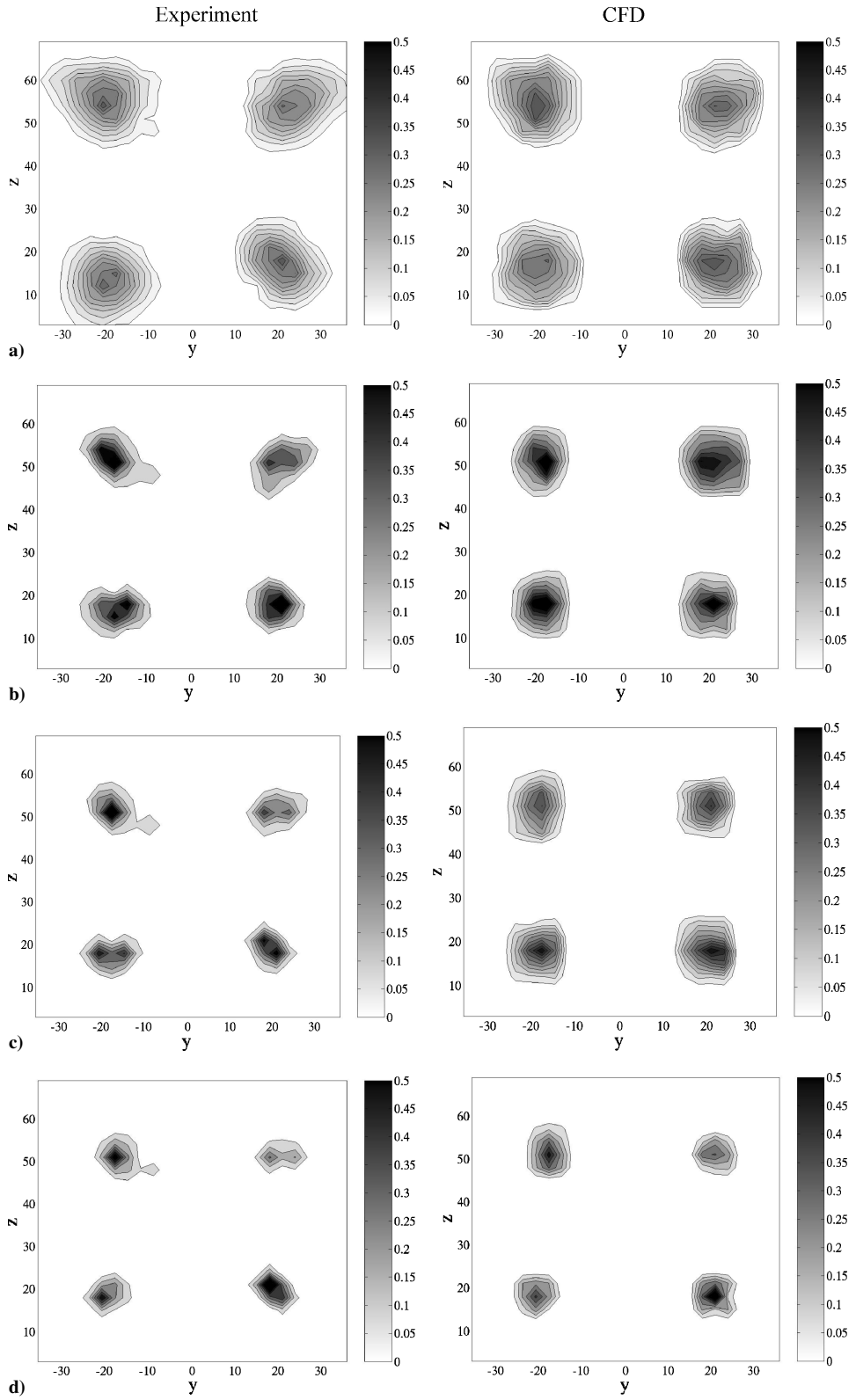

Fig. 4 Four-injector LWC experimental and numerical results for a) 100 kn and 21-μm MVD, b) 100 kn and 120-μm MVD, c) 150 kn and 120-μm MVD, and d) 200 kn and 120-μm MVD (note that units for *y* and *z* are in inches).

droplet case has peak locations that are somewhat closer to the center than that for the smaller droplets and that the predictions of these peaks are in good agreement with the experimental results (e.g., peaks generally within 1 in.). Figure 6 shows the variation of droplet cloud width averaged over all four spray clouds σ_{avg} as a function of the mean test-section velocity magnitude. It was found that increasing the test-section velocity leads to a nearly linear decrease in the single spray cloud size for the experiments (as expected from the LWC spatial distribution results). Once again, it can be noticed that predictions are in good agreement with the experiments, though some underpredictions were noted, which might be related to the fact that the experimental results were more non-Gaussian.

To further quantify the prediction capability, Table 1 shows the comparison of Gaussian fit properties averaged over all four spray bars for the condition of 150 kn and 21 μ mean volumetric diameter

droplets. It can be seen that predictions are in generally good agreement with the experiments and of the order of experimental repeatability. Table 2 shows the comparison of Gaussian properties obtained from the results of the CFD and experimental cloud LWC four-injector distributions at various speeds and droplet size. The averaged differences between experimental and computational fluid dynamics (CFD) Gaussian-fitted results for width and mean location were again less than 1 in. at all conditions. Thus, the droplet trajectory approach with a CRW model to incorporate turbulence effects can reasonably predict mean droplet diffusion and mean path (based on a Gaussian shape assumption) for these four single-injector locations.

Table 1 Comparison of Gaussian fit properties for each spray cloud averaged over all four sprays at 150 kn and MVD of 21 μm, where $|\text{exp}_1\text{-exp}_2|$ refers to the differences between two different LWC runs at the same conditions, while $|\text{CFD-exp}_{\text{avg}}|$ refers to the differences between the simulated properties and the average measured properties (from the two repeat LWC runs)

Properties	$\lvert\text{exp}_1\text{-exp}_2\rvert$	$\lvert\text{CFD-exp}_{\text{avg}}\rvert$
$\Delta\sigma_{\text{avg}}$	0.10 in.	0.45 in.
Δy_{peak}	0.27 in.	0.25 in.
Δz_{peak}	0.30 in.	0.57 in.
$\Delta L_{\text{peak}}/L_{\text{peak}}$	0.02	0.03

LWC for Cases with Baseline Nozzles

As just demonstrated, wind-tunnel aerodynamic properties and droplet sizes can play a critical role in the droplet dispersion and thus in the icing cloud uniformity. Based on the reasonable predictive

Table 2 Comparison of Gaussian fit properties between CFD and experimental values averaged over all four sprays at various speeds and droplet sizes

Properties for $\lvert\text{CFD-exp}_{\text{avg}}\rvert$	100 kn, 21-μm MVD	200 kn, 21-μm MVD	100 kn, 120-μm MVD	200 kn, 120-μm MVD
$\Delta\sigma_{\text{avg}}$	0.22 in.	0.37 in.	0.48 in.	0.41 in.
Δy_{peak}	0.72 in.	0.13 in.	0.20 in.	0.15 in.
Δz_{peak}	0.64 in.	0.20 in.	0.31 in.	0.26 in.
$\Delta L_{\text{peak}}/L_{\text{peak}}$	0.03	0.04	0.05	0.03

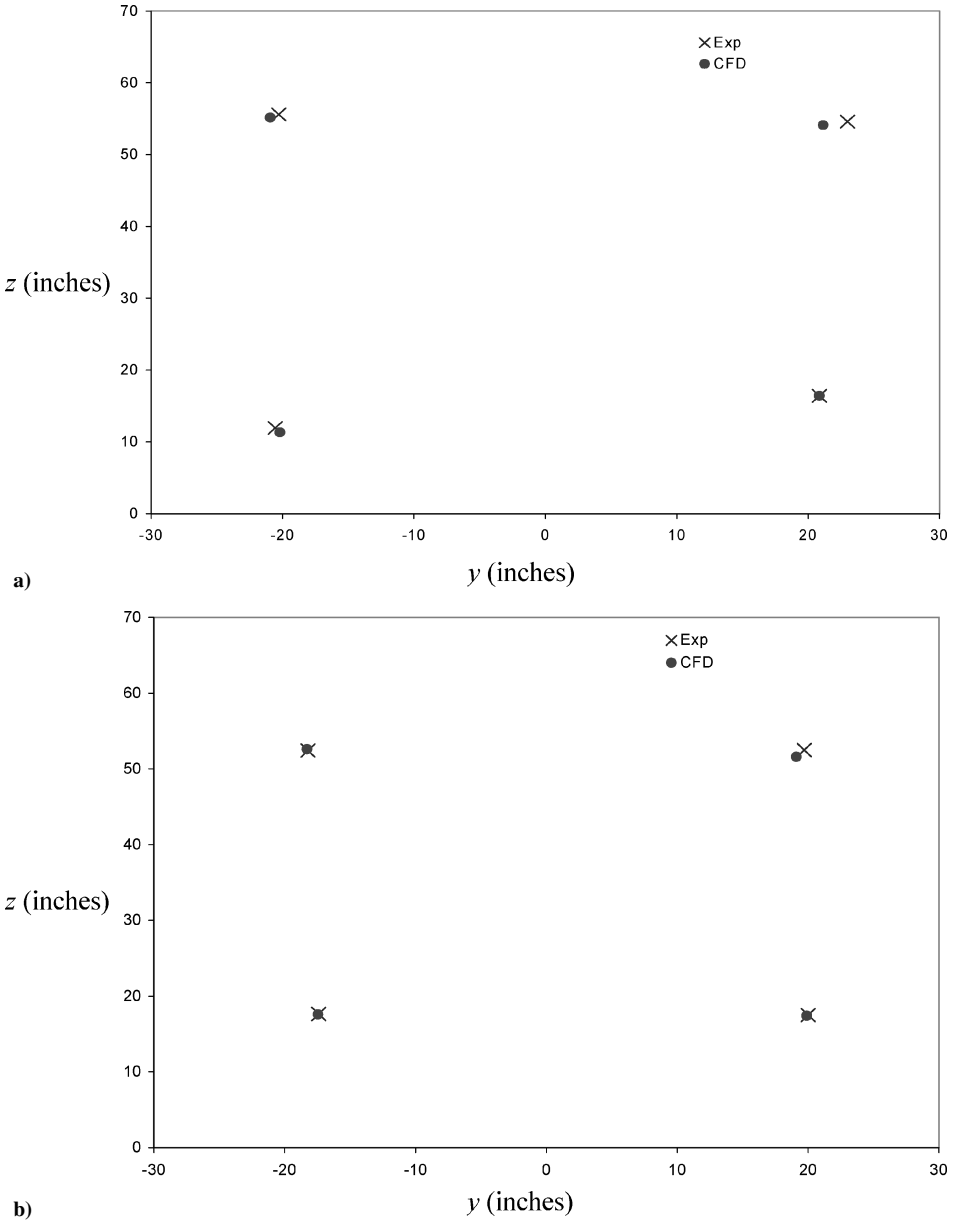

Fig. 5 Scatter plots showing y_{peak} and z_{peak} for experiments and simulations at test-section speed of 100 kn and a) 21-μm, jet air pressure of 20 psig and b) 120-μm, jet air pressure of 5 psig.

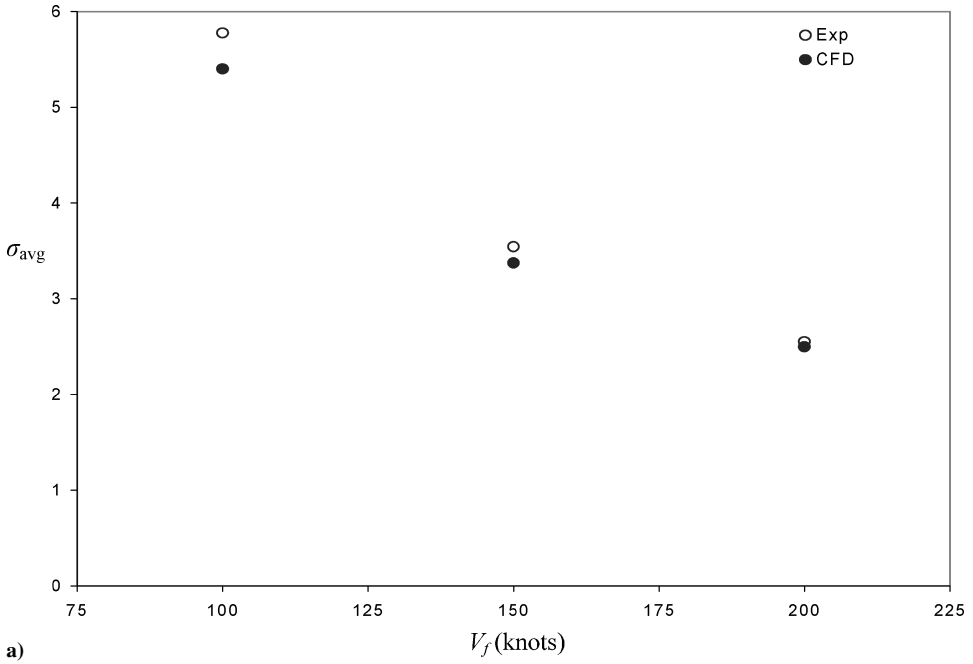

a)

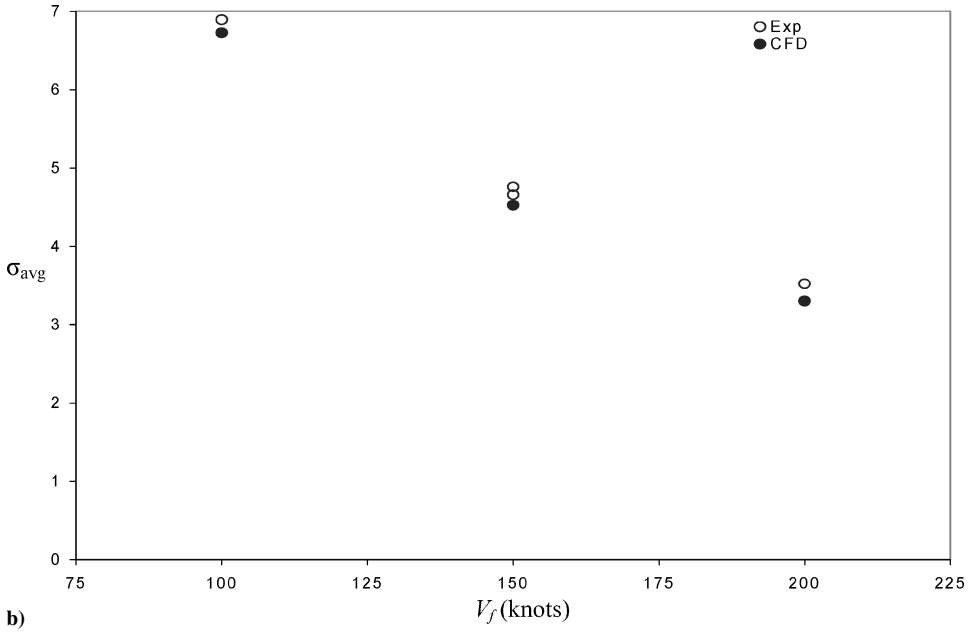

b)

Fig. 6 Scatter plots showing σ_{avg} for experiments and simulations at various test-section speeds for a) 120-μm, jet air pressure of 5 psig and b) 21-μm, jet air pressure of 20 psig.

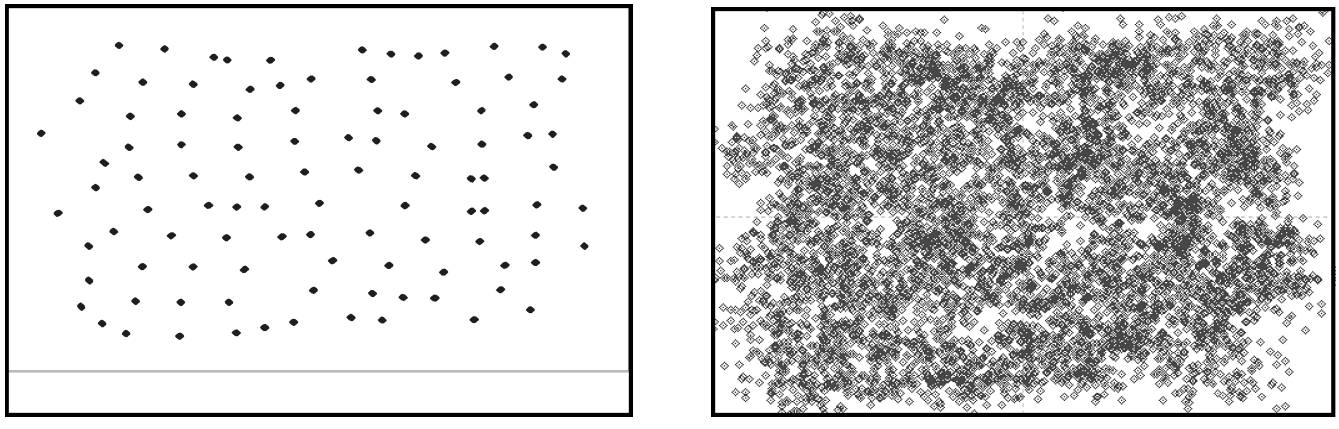

a) b)

Fig. 7 Droplet distribution in the center part of test section (width of 80 in. and height of 60 in.) for simulations: a) without turbulence and b) with turbulence.

success for the cases with four nozzles spraying, all the baseline Mod-1 nozzles (consistent with the conventional IRT operation configuration) were activated to spray in the simulation, to allow comparison with LWC test-section measurements taken by Ide and Oldenberg.[4] Figure 7 shows droplet impact location distributions in the test-section plane (bullet plots) at a test-section speed of 150 kn for two cases: one where no turbulent diffusion is included in the simulation ($\boldsymbol{u}'_f = 0$) and one where the droplet turbulence diffusion was included ($\boldsymbol{u}'_f$ based on the CRW technique). It can be seen (Fig. 7a) that when the fluctuating velocity components (i.e., turbulence values) are set to zero the particles move generally on the airflow streamline to single points in the test section (even though conical trajectories were initiated at the nozzle injection location). However, when the turbulence is taken into account (Fig. 7b), the droplets are dispersed (according to the intensity of the turbulence) and result in a much more uniform cloud formation in the test section. This comparison clearly demonstrates the importance of turbulent kinetic energy in the dispersion of particles.

Based on these droplet trajectories, the LWC distributions produced at the test section were obtained for a variety of speeds and droplet MVDs. Sample cases are shown in the following, and additional cases are available in Bhargava.[16] Figure 8 shows two measured results [a repeat experiment conducted by Ide (personal communication, 2003)] and the simulated result for the condition of 150 kn with a jet air pressure of 20 psig and a 21-μ MVD. Many of the primary features of the LWC distribution seen in the experiments are also seen in the LWC prediction: rapid drop off at the upper, lower, and left edges and peaks at (y, z) values of (−30 in., 60 in.), (−15 in., 15 in.), (−5 in., 65 in.), and (5 in., 40 in.). However, some of the predicted LWC features are not seen in the measured distributions. Similarly, some of the spatial nonuniformities seen in one of the experimental LWC distributions are

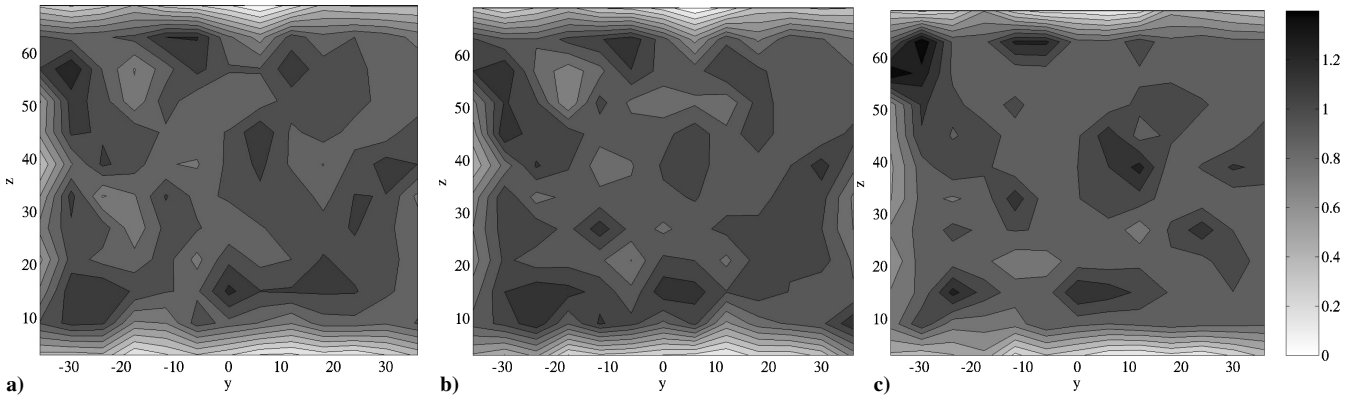

Fig. 8 LWC distribution in the test section at 150 kn with 21-μm MVD based on a) first experimental case, b) second experimental case, and c) numerical prediction.

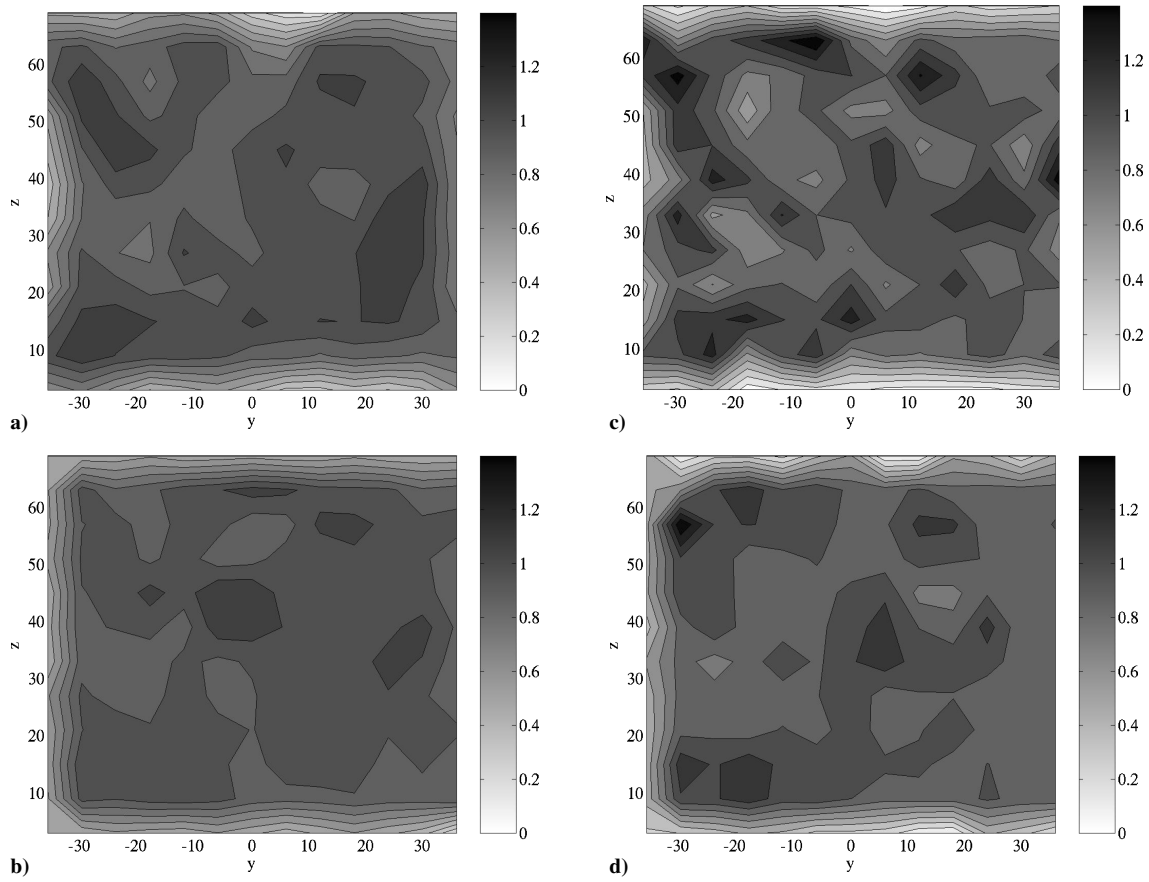

Fig. 9 LWC distribution in the test section based on a) 100 kn with 21-μm MVD experimental, b) 100 kn with 21-μm MVD numerical, c) 200 kn with 21-μm MVD experimental, and d) 200 kn with 21-μm MVD numerical.

not repeatable. This indicates that many of the differences between experiment and simulation were caused by issues of measurement repeatability. To quantify this level of repeatability, the absolute value of the difference between the two experimental LWC distributions was integrated numerically over the y-z domain, which yields $|\mathrm{LWC}_{\mathrm{exp1}} - \mathrm{LWC}_{\mathrm{exp2}}|_{\mathrm{avg}} = 0.06\mathrm{LWC}_{\mathrm{avg}}$. In comparison, the integrated difference between the average experimental and the simulated LWC profiles is $|\mathrm{LWC}_{\mathrm{exp,avg}} - \mathrm{LWC}_{\mathrm{CFD}}|_{\mathrm{avg}} = 0.07\mathrm{LWC}_{\mathrm{avg}}$. This indicates that the quantified error magnitude for the simulation is of the same order as the experimental repeatability (which in turn can be estimated as experimental uncertainty). Unfortunately, no repeatability measurements were available for the other flow speeds and droplet sizes.

Figure 9 shows the comparison between experimental and predicted LWC distributions at 100 and 200 kn. In general, the measured results indicate a significant drop off in LWC along the left, top, and bottom edges and a variety of peaks and valleys in the middle region of the icing cloud. In this middle region, there is a decreased uniformity as tunnel speed increases. The predicted LWC distributions show the same drop off in LWC near the left, top, and bottom edges and the same trend of decreasing uniformity as speed increases. However the predicted profiles tend to be more uniform than their experimental counterparts (though several of the peak features are qualitatively reproduced). The influence of speed on cloud uniformity is attributed to the decreased diffusion of the clouds from the spray of an individual nozzle (as seen in Fig. 4). In general, the comparison between predictions and experiments is most favorable at 150 kn, possibly because the LWC spatial variations are moderate, that is, not so small to be statistically unrepeatable and not so large as to be influenced by more complex flow phenomena at higher speeds.

Though not shown herein, Bhargava[16] reports that the LWC experiments and predictions with 120-μ MVD are significantly less uniform than the preceding 21-μ MVD cases. This result is also consistent with the reduced diffusion noted in Fig. 4 for the individual nozzle spray clouds as droplet size increases. Finally, Bhargava[16] also reports that the turbulence from the jets and the spray-bar wakes is important to provide reasonable fidelity of the LWC variations throughout the test section (i.e., neglecting these yielded reduced prediction fidelity). This importance of the jet and spray-bar turbulence can be expected because they more than triple the overall kinetic energy of the airflow.[7] Additional measurements of the turbulence and LWC repeatability in the facility over a larger range of flow conditions would be beneficial to further develop and validate the computational method.

Conclusions

Computational simulations of nozzle sprays in the NASA Glenn Icing Research Tunnel at various conditions were conducted to help understand the fluid physics associated with the test-section icing cloud. The computational droplet flux results at the test section were compared with measurements of the liquid water content taken at the same location. For the spray clouds emanating from four nozzles, comparisons of the computational and measured LWC results at the test section location indicate that the simulation does a reasonable job of tracking the size, strength, and location of individual nozzle clouds. In particular, comparisons of Gaussian representations of the computations and measurements show that the simulation errors in the Gaussian fit properties are of the order of the repeatability of the measured Gaussian fit properties. Results indicated that the nominal diameter of each spray decreased as test-section speed and MVD increased. For a baseline-nozzles cloud (i.e., one composed of sprays from the full complement of nozzles used for making uniform test-section LWC clouds) measurements and predictions exhibited reduced uniformity as test-section speed and MVD increased. This was successfully predicted, at least qualitatively, with the current methodology. These results suggest a relationship between spreading of individual sprays and the uniformity of the icing cloud as a function of tunnel speed and cloud MVD. In general, the LWC results from both the four-injector and all-injector cases indicate the strong importance of turbulent diffusion in spreading the droplets across the tunnel as they travel from the nozzles to the test section.

Acknowledgments

This work was supported by NASA John H. Glenn Research Center at Lewis Field. We wish to thank (alphabetically) T. Bocksell, J. Gonzales, P. Hancir, R. Ide, and J. Oldenburg for their contributions and support. Computer time was furnished by the National Center for Supercomputing Applications.

References

[1]Bragg, M. B., and Khoudadoust, A., "Study of the Droplet Spray Characteristics of a Subsonic Wind Tunnel," *Journal of Aircraft*, Vol. 32, No. 1, 1995, pp. 199–204.

[2]Hancir, P., and Loth, E., "Computations of Droplet Distribution in the IRT," AIAA Paper 99-0097, Jan. 1999.

[3]DeAngelis, B. C., Loth, E., Lankford, D., and Bartlett, C. S., "Computations of Turbulent Droplet Dispersion for Wind Tunnel Test," *Journal of Aircraft*, Vol. 34, No. 2, 1997, pp. 2130–2190.

[4]Ide, R. F., and Oldenburg, J. R., "Icing Cloud Calibration of the NASA Glenn Icing Research Tunnel," AIAA Paper 2001-0234, Jan. 2001.

[5]Irvine, T. B., Kevdzija, S. L., Sheldon, D. W., and Spera, D. A., "Overview of the Icing and Flow Quality Improvements Program for the NASA Glenn Icing Research Tunnel," AIAA Paper 2001-0229, Jan. 2001.

[6]Gonsalez, J. C., Arrington, E. A., and Curry, M. R., "Flow Quality Surveys of the NASA Glenn Icing Research Tunnel (2000 tests)," AIAA Paper 2001-0232, Jan. 2001.

[7]Bhargava, C., Loth, E., and Potapczuk, M., "Aerodynamic Simulations of the GRC Icing Research Tunnel," AIAA Paper 2003-0566, Jan. 2003.

[8]Bush, R. H., Power, G. D., and Towne, C. E., "WIND: The Production Flow Solver of NPARC Alliance," AIAA Paper 98-0935, Jan. 1998.

[9]Bocksell, T., and Loth, E., "Discontinuous and Continuous Random Walk Models for Particle Diffusion in Free-Shear Flows," *AIAA Journal*, Vol. 39, No. 6, 2001, pp. 1086–1096.

[10]Snyder, W. H., and Lumley, J. L., "Some Measurements of Particle Velocity Autocorrelation Functions in a Turbulent Flow," *Journal of Fluid Mechanics*, Vol. 48, 1971, pp. 41–71.

[11]Hinze, J. O., *Turbulence*, McGraw–Hill, New York, 1959, Chap. 5.

[12]Elghobashi, S., and Truesdell, G. C., "Direct Simulation of Particle Dispersion in a Decaying Isotropic Turbulence," *Journal of Fluid Mechanics*, Vol. 242, 1984, pp. 655–700.

[13]Loth, E., and Stedl, J., "Taylor and Lagrangian Correlations in a Turbulent Free Shear Layer," *Experiments in Fluids*, Vol. 26, Nos. 1–2, 1999, pp. 1–6.

[14]Loth, E., "Numerical Approaches to Dilute Two-Phase Flow," *Progress in Energy and Combustion Science*, Vol. 26, No. 3, 2000, pp. 161–223.

[15]Bhargava, C., Loth, E., and Potapczuk, M., "Numerical Simulation of Icing Clouds in the NASA Glenn Icing Research Tunnel," AIAA Paper 2004-0563, Jan. 2004.

[16]Bhargava, C., "Computations of the Droplet Distributions in the NASA Glenn Icing Research Tunnel," M.S. Thesis, Dept. of Aerospace Engineering, Univ. of Illinois at Urbana–Champaign, IL, Sept. 2003.